ACS MATERIALS LETTERS

www.acsmaterialsletters.org

Identifying $\pi-\pi$ and $\pi-$Lone Pair Interactions in a Single-Molecule Junction

Yanxia Xu,[#] Jie Hao,[#] Hongyu Ju, Suhang He, Jinying Wang,* Chuancheng Jia,* and Xuefeng Guo*

Cite This: *ACS Materials Lett.* 2024, 6, 1961−1967

Read Online

ACCESS | Metrics & More | Article Recommendations | Supporting Information

ABSTRACT: **Noncovalent interactions are essential in determining molecular conformations and assembly architectures, serving as key factors in regulating material properties. Achieving a comprehensive understanding and precise control of these interactions is crucial in molecular design and the development of functional devices. Here, we utilize scanning tunneling microscopic break junction measurements and first-principles calculations to identify $\pi-\pi$ and $\pi-$lone pair ($\pi-$lp) interactions within diphenyl disulfide derivatives at the single-molecule level. The competition between $\pi-\pi$ and $\pi-$lp interactions regulates molecular conformation and conductance, leading to switching between high- and low-conductance states. Specifically, $\pi-\pi$ interactions promote the high-conductance state, while $\pi-$lp interactions drive the molecule into a low-conductance state. Chemical modifications provide efficient methods to adjust $\pi-\pi$ and $\pi-$lp interactions. These findings not only reveal the underlying mechanism of how $\pi-\pi$ and $\pi-$lp interactions influence molecular conformation and induce the stereoelectronic effect but also offer a novel approach for creating practical devices.**

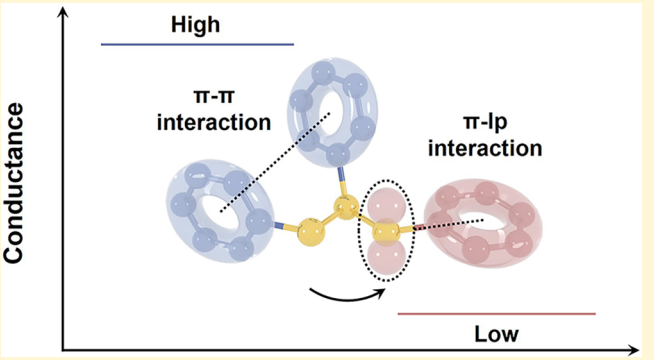

Noncovalent interactions are the subtle but fundamental forces that govern the structure and properties of matter, playing a crucial role in molecular recognition,[1,2] catalyst design,[3,4] and the assembly of larger molecular structures.[5,6] Within the realm of noncovalent interactions, which encompass hydrogen bonds, van der Waals forces, ionic interactions, and π-involved interactions,[7] the significance of $\pi-\pi$[8,9] and $\pi-$lone pair ($\pi-$lp) interactions[10,11] cannot be overstated. $\pi-\pi$ and $\pi-$lp interactions significantly affect intramolecular and intermolecular structures associated with aromatic rings, double bonds, and other conjugated groups. Effective chiral recognitions in the dihydroxy-based kinetics have been successfully achieved through the combination of $\pi-\pi$ and $\pi-$lp interactions in previous studies.[12] By manipulating and exploiting these interactions, it is possible to design and modify molecular conformation[13] and chemical processes.[14,15]

To date, the precise recognition and characterization of $\pi-\pi$ and $\pi-$lp interactions remain a formidable challenge. This is ascribed to the possible competition and synergetic cooperation that can exist between the relatively weak noncovalent π interactions and other types of interactions. In addition, the presence of molecular ensembles and disordered accumulation greatly hampers the precise identification of $\pi-\pi$ and $\pi-$lp interactions.[7,16] The emergence of single-molecule techniques, especially single-molecule electrical measurement,[17−20] opens up a new avenue in probing and quantifying the π-involved interactions,[21−24] due to the strong correlation between molecular conformation and conductance such as stereoelectronic effect.[25−27] For example, the stereoelectronic effect of biphenyl is investigated using the graphene-based single-molecule junction.[26] The twisting of phenyl rings causes various microstates with different conjugation degrees, which results in stochastic switching between high- and low-conductance states. Through precise manipulation of the π-stacked molecular dimers, the destructive quantum interference can be turned on or off.[23] Although $\pi-\pi$ and $\pi-$lp interactions have been well studied theoretically,[8,11,28] there is still a deficiency in the precise experimental characterization and control of these subtle interactions.

In this study, we employ the scanning tunneling microscope break junction (STM-BJ) technique alongside theoretical calculations to track $\pi-\pi$ and $\pi-$lp interactions within phenyl

Received: February 23, 2024
Revised: March 23, 2024
Accepted: April 9, 2024
Published: April 12, 2024

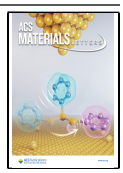

https://doi.org/10.1021/acsmaterialslett.4c00402
ACS Materials Lett. 2024, 6, 1961−1967

disulfide derivatives. The impact of the competition between $\pi-\pi$ and $\pi-$lp interactions on the molecular conformation and electronic properties is unveiled. Chemical modifications are employed to efficiently adjust $\pi-\pi$ and $\pi-$lp interactions and to change the molecular conformation and device conductance. These findings offer valuable insights for a profound understanding and precise control of the molecular conformation and electronic behavior, promoting the development of molecular electronics and supramolecular science.

Benzene serves as the fundamental model system for investigating π electrons, while disulfide bonds, providing lone pairs of electrons, are essential in various organic electronic devices[29,30] and biological processes.[31] The combination of benzene and disulfide bonds results in phenyl disulfide, possessing multiple noncovalent interactions such as $\pi-\pi$ and $\pi-$lp interactions. As shown in Figure 1A and Figure S1, the orbital analysis reveals a distinct hybridization between π and lp electrons in the phenyl and disulfide groups, resulting in unique occupied orbitals in diphenyl disulfide (M1). Therefore, phenyl disulfide derivatives, extensively studied in fields like organic chemistry, biochemistry, and materials science, offer an excellent platform to examine how these subtle π-involved interactions influence molecular conformation and electronic properties. Through a relaxation potential energy surface (PES) scan of M1 and structural optimization, we have identified two distinct stable conformations labeled as State 1 and State 2 (Figure 1B), respectively. The primary structural difference between State 1 and State 2 is evident in the dihedral angles of CSSC and SSCC. Specifically, the SSCC dihedral angle in State 1 measures ~85°, while in State 2, it is ~22°. This variance causes the benzene rings and disulfide bond in State 1 to tend toward perpendicularity, whereas in State 2, they tend to be planar. Consequently, the distance between the two phenyl rings in State 1 (~0.49 nm) is shorter than that in State 2 (~0.58 nm). The disparity in structure results in notable differences in the electronic states of States 1 and 2. Density functional theory (DFT) calculations indicate

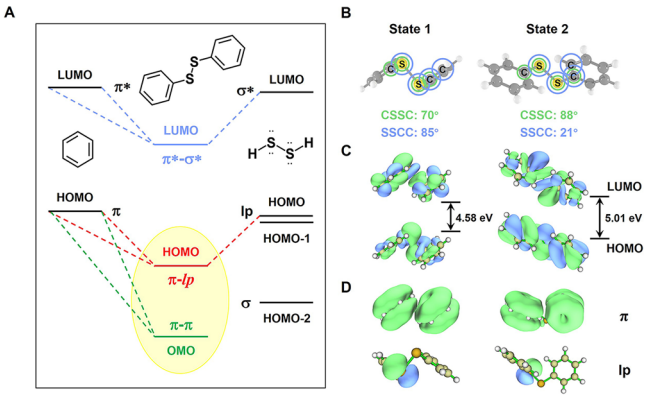

Figure 1. Theoretical calculation of stable conformations, molecular orbitals, and noncovalent $\pi-\pi$ and $\pi-$lp interactions in M1. (A) Molecular orbital energy level of M1. OMO means the other occupied molecular orbital. (B) Two stable molecular conformations of M1, that is, State 1 and State 2, respectively. The green circles refer to the CSSC dihedral angles, and the purple circles refer to the SSCC dihedral angles. (C) Calculated frontier molecular orbital diagrams for States 1 and 2 in M1. (D) Electron localization function (ELF) maps of π orbitals (top) and localized nature bond orbitals of lp electrons (bottom) for State 1 and State 2 in M1.

that the energy gap of State 1 is considerably smaller than that of State 2. Moreover, the lowest unoccupied molecular orbitals (LUMO), highest occupied molecular orbitals (HOMO), and other occupied molecular orbitals (OMO) for both States 1 and 2 (Figure 1C) are consistent with our initial orbital hybridization analysis. In comparison to State 2, the S electron component of HOMO in State 1 significantly outweighs the π electrons of the phenyl ring (Figure 1C), suggesting a weaker $\pi-$lp hybridization, while the $\pi-\pi$ overlap of HOMO−1 is stronger in State 1 than that in State 2 (Figure S1). To explore the distinct orbital interactions in M1, we adopted a multifunctional wavefunction analyzer (Multiwfn) to extract the π and lp electrons from the orbitals in State 1 and State 2 (Figure 1D), respectively. We also employed the second-order perturbation theory in natural bond orbital (NBO)[32] for quantitative analyses of the relevant orbital interactions. Evident overlap between the π orbitals in the phenyl rings of State 1 results in a robust $\pi-\pi$ interaction. In contrast, State 2 exhibits a strong $\pi-$lp interaction (Figure S2). This interaction leads to a substantial reduction in the energy of State 2 by ~17.6 kcal/mol, in comparison with the comparatively smaller energy reduction of ~5.8 kcal/mol in State 1. These results highlight the competition between $\pi-\pi$ and $\pi-$lp interactions in M1, altering the distribution of the molecular orbitals and structural stability. This alteration potentially leads to a stereoelectronic effect, providing a basis for recognizing and characterizing $\pi-\pi$ and $\pi-$lp interactions by using the single-molecule break junction technique.

To confirm that the competition between $\pi-\pi$ and $\pi-$lp interactions induces a stereoelectronic effect, we investigated the charge transport properties of M1 by integrating theoretical calculations with single-molecule electrical measurements. DFT combined with the nonequilibrium Green's function (NEGF) method is applied to compute the transport properties of State 1 and State 2 devices (Figure 2A) under a zero-bias voltage. The transmission spectrum (Figure 2B) reveals that the conductance of State 1 is significantly higher than that of State 2 near the Fermi level, potentially due to the stronger $\pi-\pi$ interaction in State 1 in comparison with that in State 2. The charge transports through States 1 and 2 are primarily influenced by the perturbed HOMOs (p-HOMO) and are denoted as p-H1 and p-H2, respectively. Their transmission paths[33,34] indicate that in p-H2, both the benzene ring and S atoms participate in electron transmission. In contrast, the transmission is more concentrated through the S atoms in p-H1. This observation aligns with their HOMO characteristics, supporting the finding that the $\pi-$lp coupling of State 2 is stronger than that of State 1 (Figure 2C). All above results suggest that the interplay between $\pi-\pi$ and $\pi-$lp interactions in States 1 and 2 affects their charge transport properties.

To verify and track the stereoelectronic effect induced by $\pi-\pi$ and $\pi-$lp interactions, we used the STM-BJ technique to characterize the charge transport properties of M1 at the single-molecule level. Specifically, a single-molecule junction (Figure 2A) can be formed by trapping the target molecule M1 between the electrode gaps through the Au−S coordination bond. As the Au STM tip moves upward, the single-molecule junction is disrupted, completing one of the sampling events. Typical conductance traces (Figure 2D) exhibit two distinct conductance plateaus, high-conductance (G_H) and low-conductance (G_L) states, which can appear individually or simultaneously. Over 5000 individual conductance−distance

https://doi.org/10.1021/acsmaterialslett.4c00402
ACS Materials Lett. 2024, 6, 1961−1967

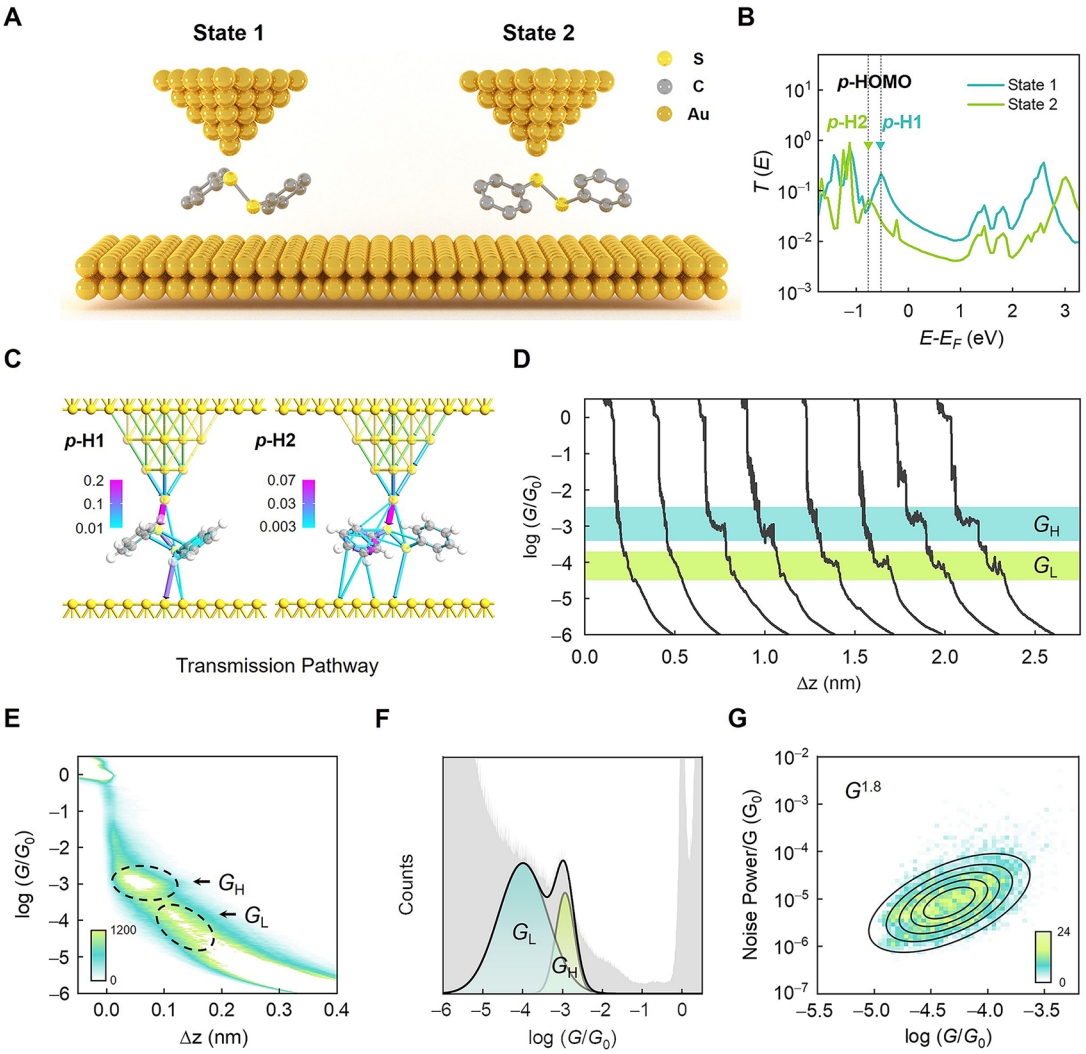

Figure 2. Charge transport properties of M1 junctions. (A) Schematic of the molecular conductance measurement via the STM-BJ technique. Yellow atom, sulfur; gray atom, carbon; golden atom, gold. Hydrogen atoms are omitted here. (B) Calculated transmission spectra for State 1 and State 2. (C) Transmission pathways for State 1 and State 2 based M1 junctions at the energy level of *p*-H1 and *p*-H2. The charge transport pathways are represented by arrows, with larger arrows indicating the higher possibility of charge transport. The color bar represents the values of local bond contributions along the transport pathway. (D) Typical individual conductance traces via STM-BJ measurements in which the first two represent tunneling decay without target molecules and others are for M1 junctions. (E) 2D conductance−distance histograms of M1. The color bar indicates the number of counts. (F) 1D conductance histograms of M1. Peak centers are labeled by Gaussian fitting, which displays a bistable conductance signature. (G) 2D histograms of normalized flicker noise power versus average conductance for M1 junctions corresponding to the G_L state.

traces are compiled to create a 2D conductance−distance histogram for M1 (Figure 2E), revealing two conductance density clouds corresponding to the G_H and G_L states. For quantitative analysis, 1D conductance histograms are plotted (Figure 2F), with the conductance peaks fitted by using Gaussian functions. The G_H peak for M1 is located around $\sim 10^{-2.9}$ G_0 (≈97.6 nS), while the G_L peak is distributed at $\sim 10^{-4.0}$ G_0 (≈7.8 nS), where G_0 represents quantum conductance ($2e^2/h$, 77.5 μS).[35] The value of the G_H peak is approximately 1 order of magnitude larger than that of G_L, consistent with the calculated conductance difference between State 1 and State 2. The relative stretching displacements corresponding to the G_H and G_L states in M1 are shown in Figure S3.

To confirm that G_H and G_L originate from States 1 and 2, respectively, we need to rule out the possibility of S−S bond breaking. During the single-molecule conductance measurements, both G_H and G_L plateaus nearly disappear (Figure S4) after adding 0.01 mM saturated tris(2-carboxyethyl)phosphine hydrochloride (TCEP) solutions within propylene carbonate into the M1 solution to break S−S bonds.[36] In addition, the conductance distributions of G_H and G_L vary little under different concentrations of M1, implying no formation of M1 dimers and suggesting that the influence of intermolecular interactions on the charge transport of M1 molecules is minimal (Figure S5). To exclude the possibility that M1 forms molecular junctions with benzene rings as the anchoring groups, we conducted STM-BJ measurements of 1,2-diphenylethane under the same conditions as M1. The 2D conductance−distance histogram and 1D conductance histogram (Figure S6) of 1,2-diphenylethane do not exhibit obvious conductance characteristics. Therefore, the likelihood of M1 forming molecular junctions with benzene rings as the anchoring groups is very low. Thus, it is reasonable to infer

https://doi.org/10.1021/acsmaterialslett.4c00402
ACS Materials Lett. 2024, 6, 1961−1967

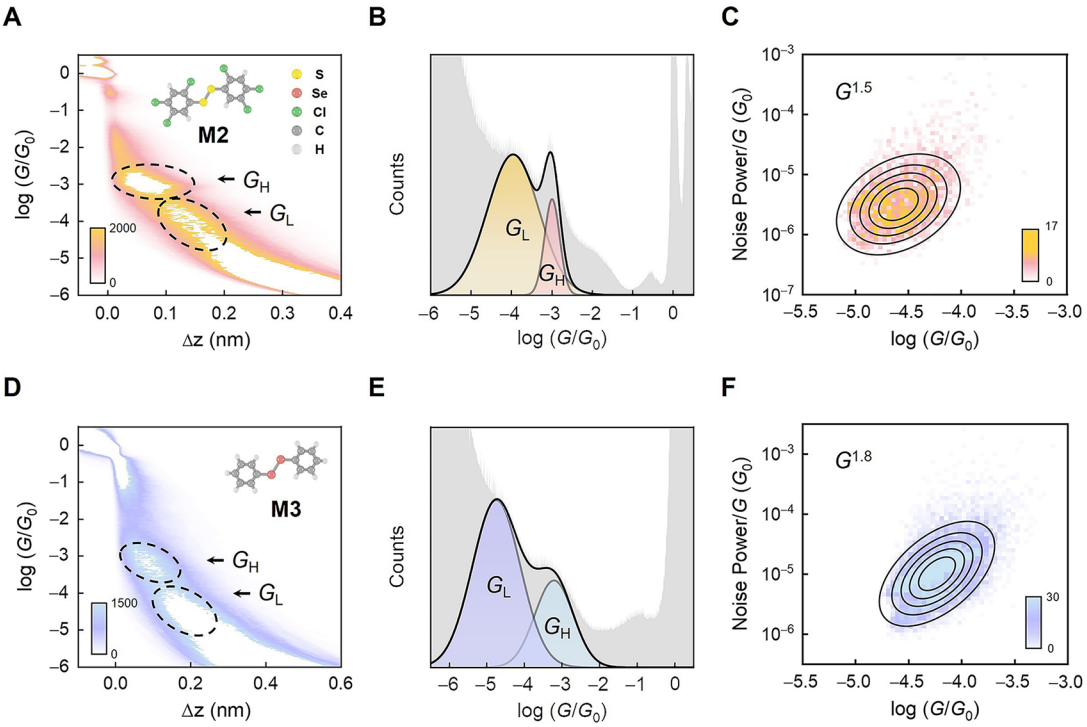

Figure 3. Break junction measurements of M2 and M3 molecular junctions. (A,D) 2D conductance−distance histograms of M2 (A) and M3 (D), respectively, where yellow atoms are sulfur, pink atoms selenium, green atoms chlorine, gray atoms carbon, and white atom hydrogen. (B,E) 1D conductance histograms of M2 (B) and M3 (E). (C,F) 2D histograms of normalized flicker noise power versus average conductance for M2 (C) and M3 (F) junctions.

that the G_H and G_L states arise from the two conformational isomers of M1, specifically, State 1 and State 2, respectively. Furthermore, the charge transport mechanism for M1 is probed through flicker noise analysis.[37−39] The noise power of G_L, referring to State 2, is $G^{1.8}$ (Figure 2G), indicating that through-space electronic couplings or noncovalent contacts mainly participate in the charge transport, aligning with the calculated transport pathways in Figure 2C. Flicker noise analysis of the G_H state cannot be performed because the G_H state jumps to the G_L state too quickly. Corresponding hovering data of G_L are shown in Figure S7.

After verifying the stereoelectronic effect caused by $\pi-\pi$ and π−lp interactions in M1, we proposed two approaches to modifying these interactions. One approach involves enhancing the $\pi-\pi$ interaction by introducing the electron-withdrawing Cl atoms,[9] while the other approach aims to increase the π−lp interaction by replacing the S−S bond with the Se−Se bond (Figure S2), corresponding to bis(2,4,5-trichlorophenyl) disulfide (M2) and diphenyl diselenide (M3) systems, respectively. We conducted single-molecule conductance measurements of M2 and M3 under the same conditions as those for M1. The 2D (Figure 3A) and 1D (Figure 3B) conductance histograms of M2 exhibit two distinct conductance peaks at around $\sim 10^{-3.0}$ G_0 (≈77.5 nS; G_H) and $\sim 10^{-4.0}$ G_0 (≈7.9 nS; G_L), respectively. M3 shows two conductance states (Figure 3D,E) located at $\sim 10^{-3.2}$ G_0 (≈48.9 nS; G_H) and $\sim 10^{-4.7}$ G_0 (≈1.55 nS; G_L), respectively. The relative displacement distributions of G_H and G_L for M2 and M3 are shown in Figure S8, and typical conductance−displacement traces are shown in Figure S9. To confirm the correspondence between the conductance states and molecular configurations in M2 and M3, we also calculated the zero-bias transmission properties for their molecular devices with different molecular conformations: State 1′ and State 2′ in M2 and State 1″ and State 2″ in M3, respectively. The transmission spectra and transmission pathways (Figure S9) also show similar stereoelectronic effects in the M1 system, where stronger $\pi-\pi$ interactions dominate in the G_H state, while π−lp interactions take precedence in the G_L state. Flicker noise analysis of the G_L states in M2 and M3 junctions reveal a slight decrease in the noise power scale of M2 from $G^{1.8}$ to $G^{1.5}$ (Figure 3C), whereas that of M3 remains unchanged (Figure 3F). This implies that the introduction of Cl in M2 increases the noncovalent interaction between M2 and Au substrate.[40] In addition, the noise power scale of G_H for M2 is $G^{1.7}$ (Figure S10), indicating that the charge transport of both States 1′ and 2′ involves through-space electronic couplings. The 2D conductance−time histograms of G_L for M2 and M3 are shown in Figure S11.

To uncover a general relation between $\pi-\pi$ and π−lp interactions and molecular conformations, we summarized the main structural features of the CSSC and SSCC dihedral angles in M1, M2, M3 and M4 as well as their $\pi-\pi$ and π−lp interactions together (Figure 4A,B and Figure S2). The $\pi-\pi$ interaction dominates in States 1, 1′, 1″, and 1‴ and exhibits a strong correlation with the CSSC dihedral angle in a monotonic manner. The stronger the $\pi-\pi$ interaction, the smaller the CSSC angle (Figure 4A). However, in States 2, 2′, 2″, and 2‴, the SSCC dihedral angle is mainly influenced by the π−lp interaction, where the reduction in the π−lp interaction leads to an increase in the SSCC angle (Figure 4B). These straightforward relationships between noncovalent interactions and molecular conformational features align with our intuitive expectation and can be readily applied to other systems. In contrast, the variations in the CSSC angle in the G_L state and the SSCC angle in the G_H state do not correspond to

https://doi.org/10.1021/acsmaterialslett.4c00402
ACS Materials Lett. 2024, 6, 1961−1967

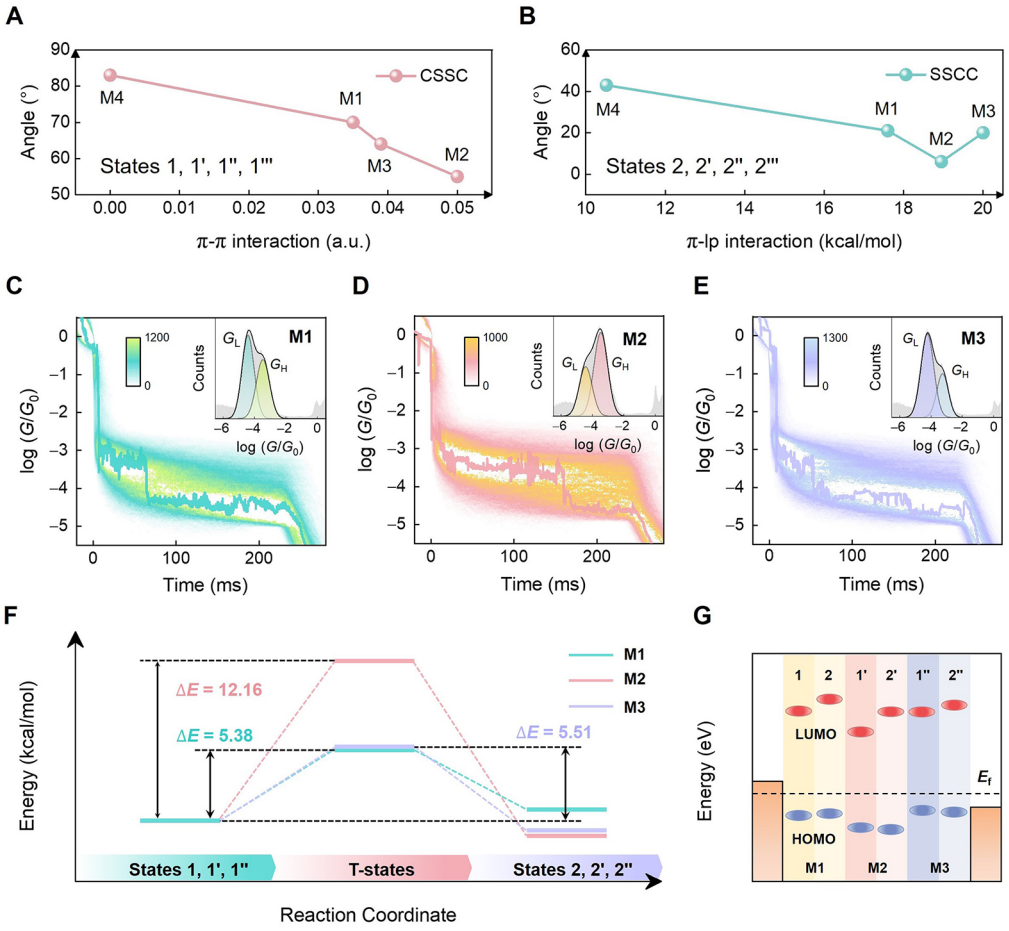

Figure 4. Relationship between $\pi-\pi$ and π−lp interactions and molecular conformation. (A) Variation of the CSSC dihedral angle with respect to $\pi-\pi$ interactions in States 1, 1′, 1″, 1‴ of M1−M4. (B) Variation of the SSCC dihedral angle with respect to π−lp interactions in States 2, 2′, 2″, 2‴ of M1−M4. The quantitative analysis of $\pi-\pi$ and π−lp interactions in phenyl disulfide derivatives (M1−M4) is shown in the Supporting Information. (C−E) 2D conductance−time histograms for M1 (C), M2 (D), and M3 (E), in which the typical individual trace is marked. The insets show the 1D conductance histograms of M1 (C), M2 (D), and M3 (E), in which peak centers are labeled by Gaussian fitting. (F) Calculated energies of two stable states and the transition states for M1−M3. (G) Molecular frontier orbital levels of M1−M3, respectively.

dominant interactions and appear to be quite irregular (Figure S2). These results confirm that the stereoelectronic effect of disulfide derivatives is determined by the competing $\pi-\pi$ and π−lp interactions. Both interactions can stabilize molecules, with $\pi-\pi$ interactions enhancing the stability of G_H states (States 1, 1′, 1″), while π−lp interactions play a crucial role in stabilizing G_L states (States 2, 2′, 2″).

To investigate the transformation kinetics of conformational isomerism, we used the hovering mode in the STM-BJ equipment to maintain the junction elongation for 200 ms after forming the molecular junction. Conductance−time traces, up to 5000 for M1, M2, and M3, are collected to construct the 2D conductance−time histograms (Figure 4C−E) at a bias of 100 mV, respectively. Irreversible jumping from the G_H state to the G_L state is observed for each junction (see typical individual traces in Figure 4C−E), indicating conformational transitions from State 1 (1′, 1″) to State 2 (2′, 2″). The mean dwell time of the G_H state for M1 and M3 junctions is shorter than that of the corresponding G_L state (see the insets of 1D conductance histograms in Figures 4C−E), but M2 junctions show the opposite result. To understand the isomerization process, we calculated the energies of stable conformations and transition states for M1, M2, and M3 molecules (Figure 4F). M2 has a higher transition energy from State 1′ to State 2′ (≈12.16 kcal mol^{-1}) than M1 (≈5.38 kcal mol^{-1}) and M3 (≈5.51 kcal mol^{-1}) cases, well explaining why M2 has the longest mean dwell time. The larger the transition energy barrier, the more difficult the conformation transition becomes, leading to a longer mean dwell time. Conversely, the smaller the transition energy barrier, the easier the conformation transition becomes, resulting in a shorter mean dwell time. However, the conformational transition pathway of free molecules does not readily explain the irreversible transition from the G_H state to the G_L state observed in hover measurements. This phenomenon may be attributed to the hindrance of the reverse reaction by the Au−S coordination bond. Furthermore, we also summarized the relationship between the molecular energy levels and orbital interactions in Figure 4G. The $\pi-\pi$ interaction-favored states (States 1, 1′, 1″) always have a smaller HOMO−LUMO energy gap compared to the corresponding π−lp interaction-preferred states (States 2, 2′, 2″). By introduction of the electron-withdrawing Cl groups in M2, the HOMO and LUMO energy levels shift downward. The HOMO−LUMO energy gap reduces in M3 due to enhanced π−lp and $\pi-\sigma^*$ interactions by replacing the S−S bond with the Se−Se bond. These chemical modifications

https://doi.org/10.1021/acsmaterialslett.4c00402
ACS Materials Lett. 2024, 6, 1961−1967

change not only molecular orbitals but also the molecular conformation stability and transitions by influencing the $\pi-\pi$ and $\pi-$lp interactions.

In summary, we explore the impact of $\pi-\pi$ and $\pi-$lp interactions on molecular configurations and transport properties at the single-molecule level. Both experimental and theoretical results consistently demonstrate that the stereoelectronic effect induced by molecular conformational transitions is primarily influenced by the competing $\pi-\pi$ and $\pi-$lp interactions. We identify two distinct conductance states and their switching mechanisms, where $\pi-\pi$ interactions promote the high-conductance state while $\pi-$lp interactions drive the molecule into the low-conductance state. Chemical modifications, such as introducing electron-withdrawing Cl groups and substituting Se−Se bonds, have been proven to be efficient methods for tuning $\pi-\pi$ and $\pi-$lp interactions, thereby altering the molecular conformation and device conductance. Our findings provide a comprehensive understanding of the stereoelectronic effect and the role of noncovalent interactions, offering a novel strategy for constructing single-molecule bistate switching devices toward real applications.

■ ASSOCIATED CONTENT

Supporting Information

The Supporting Information is available free of charge at https://pubs.acs.org/doi/10.1021/acsmaterialslett.4c00402.

STM-BJ measurements, flicker noise analysis, theoretical calculations, NBO calculations, calculated molecular orbital diagrams, quantitative analysis of noncovalent interactions, auxiliary experiments of M1, auxiliary experiments of M2 and M3 (PDF)

■ AUTHOR INFORMATION

Corresponding Authors

Jinying Wang − *Network for Computational Nanotechnology, School of Electrical and Computer Engineering, Purdue University, West Lafayette, Indiana 47907, United States*; Email: wang4205@purdue.edu

Chuancheng Jia − *Center of Single-Molecule Sciences, Institute of Modern Optics, Frontiers Science Center for New Organic Matter, Tianjin Key Laboratory of Micro-scale Optical Information Science and Technology, College of Electronic Information and Optical Engineering, Nankai University, Tianjin 300350, P. R. China*; Email: jiacc@nankai.edu.cn

Xuefeng Guo − *Center of Single-Molecule Sciences, Institute of Modern Optics, Frontiers Science Center for New Organic Matter, Tianjin Key Laboratory of Micro-scale Optical Information Science and Technology, College of Electronic Information and Optical Engineering, Nankai University, Tianjin 300350, P. R. China; Beijing National Laboratory for Molecular Sciences, National Biomedical Imaging Center, College of Chemistry and Molecular Engineering, Peking University, Beijing 100871, P. R. China*; orcid.org/0000-0001-5723-8528; Email: guoxf@pku.edu.cn

Authors

Yanxia Xu − *Center of Single-Molecule Sciences, Institute of Modern Optics, Frontiers Science Center for New Organic Matter, Tianjin Key Laboratory of Micro-scale Optical Information Science and Technology, College of Electronic Information and Optical Engineering, Nankai University, Tianjin 300350, P. R. China*; orcid.org/0000-0001-5339-4638

Jie Hao − *Center of Single-Molecule Sciences, Institute of Modern Optics, Frontiers Science Center for New Organic Matter, Tianjin Key Laboratory of Micro-scale Optical Information Science and Technology, College of Electronic Information and Optical Engineering, Nankai University, Tianjin 300350, P. R. China*

Hongyu Ju − *School of Pharmaceutical Science and Technology, Tianjin University, Tianjin 300072, P. R. China*; orcid.org/0009-0001-5689-0597

Suhang He − *Center of Single-Molecule Sciences, Institute of Modern Optics, Frontiers Science Center for New Organic Matter, Tianjin Key Laboratory of Micro-scale Optical Information Science and Technology, College of Electronic Information and Optical Engineering, Nankai University, Tianjin 300350, P. R. China*

Complete contact information is available at: https://pubs.acs.org/10.1021/acsmaterialslett.4c00402

Author Contributions

#These authors contributed equally to this work. X.G., C.J., and J.W. conceived the idea for the paper. Y.X. carried out the experimental measurements. J.H. and J.W. performed the theoretical calculations. X.G., C.J., J.W., Y.X., J.H., H.J., and S.H. analyzed the data and wrote the paper. All the authors discussed the results and commented on the manuscript. CRediT: **Yanxia Xu** conceptualization, data curation, investigation, methodology, validation, writing-original draft, writing-review & editing; **Jie Hao** conceptualization, data curation, investigation, methodology, validation; **Hongyu Ju** conceptualization, investigation, writing-review & editing; **Suhang He** conceptualization, investigation, writing-review & editing; **Jinying Wang** conceptualization, investigation, methodology, validation, writing-review & editing; **Chuancheng Jia** conceptualization, investigation, methodology, validation, writing-review & editing; **Xuefeng Guo** conceptualization, investigation, methodology, validation, writing-review & editing.

Notes

The authors declare no competing financial interest.

■ ACKNOWLEDGMENTS

The authors acknowledge primary financial supports from the National Key R&D Program of China (2021YFA1200102, 2021YFA1200101, and 2022YFE0128700), the National Natural Science Foundation of China (22173050, 22150013, 21727806, and 21933001), the New Cornerstone Science Foundation through the XPLORER PRIZE, the Natural Science Foundation of Beijing (2222009), Beijing National Laboratory for Molecular Sciences (BNLMS202105), the Fundamental Research Funds for the Central Universities (63223056), and "Frontiers Science Center for New Organic Matter" at Nankai University (63181206).

■ REFERENCES

(1) Hunter, C. A. Meldola lecture. The Role of Aromatic Interactions in Molecular Recognition. *Chem. Soc. Rev.* **1994**, *23*, 101−109.

(2) Pérez, E. M.; Capodilupo, A. L.; Fernández, G.; Sánchez, L.; Viruela, P. M.; Viruela, R.; Ortí, E.; Bietti, M.; Martín, N. Weighting Non-Covalent Forces in the Molecular Recognition of C_{60}. Relevance

of Concave-Convex Complementarity. *Chem. Commun.* **2008**, *38*, 4567−4569.
(3) Neel, A. J.; Hilton, M. J.; Sigman, M. S.; Toste, F. D. Exploiting Non-Covalent π Interactions for Catalyst Design. *Nature* **2017**, *543*, 637−646.
(4) Proctor, R. S.; Colgan, A. C.; Phipps, R. J. Exploiting Attractive Non-Covalent Interactions for the Enantioselective Catalysis of Reactions Involving Radical Intermediates. *Nat. Chem.* **2020**, *12*, 990−1004.
(5) Rest, C.; Kandanellia, R.; Fernández, G. Strategies to Create Hierarchical Self-Assembled Structures via Cooperative Non-covalent Interactions. *Chem. Soc. Rev.* **2015**, *44*, 2543−2572.
(6) Song, S.; Wang, L.; Su, J.; Xu, Z.; Hsu, C.; Hua, C.; Lyu, P.; Li, J.; Peng, X.; Kojima, T.; et al. Manifold Dynamic Non-Covalent Interactions for Steering Molecular Assembly and Cyclization. *Chem. Sci.* **2021**, *12*, 11659−11667.
(7) Haque, A.; Alenezi, K. M.; Khan, M. S.; Wong, W.; Raithby, P. R. Non-Covalent Interactions (NCIs) in π-Conjugated Functional Materials: Advances and Perspectives. *Chem. Soc. Rev.* **2023**, *52*, 454−472.
(8) Grimme, S. Do Special Noncovalent π-π Stacking Interactions Really Exist? *Angew. Chem., Int. Ed.* **2008**, *47*, 3430−3434.
(9) Martinez, C. R.; Iverson, B. L. Rethinking the Term "pi-Stacking. *Chem. Sci.* **2012**, *3*, 2191−2201.
(10) Egli, M.; Sarkhel, S. Lone Pair-Aromatic Interactions: To Stabilize or Not to Stabilize. *Acc. Chem. Res.* **2007**, *40*, 197−205.
(11) Mooibroek, T. J.; Gamez, P.; Reedijk, J. Lone Pair-π Interactions: A New Supramolecular Bond? *CrystEngComm* **2008**, *10*, 1501−1515.
(12) Jin, M.; Zhen, Q.; Xiao, D.; Tao, G.; Xing, X.; Yu, P.; Xu, C. Engineered Non-Covalent π Interactions as Key Elements for Chiral Recognition. *Nat. Commun.* **2022**, *13*, 3276.
(13) Sharber, S. A.; Baral, R. N.; Frausto, F.; Haas, T. E.; Müller, P.; Thomas, S. W. Substituent Effects that Control Conjugated Oligomer Conformation through Non-Covalent Interactions. *J. Am. Chem. Soc.* **2017**, *139*, 5164−5174.
(14) DiLabio, G. A.; Johnson, E. R. Lone Pair-π and π-π Interactions Play an Important Role in Proton-Coupled Electron Transfer Reactions. *J. Am. Chem. Soc.* **2007**, *129*, 6199−6203.
(15) Krenske, E. H.; Houk, K. N. Aromatic Interactions as Control Elements in Stereoselective Organic Reactions. *Acc. Chem. Res.* **2013**, *46*, 979−989.
(16) Mati, I. K.; Cockroft, S. L. Molecular Balances for Quantifying Non-Covalent Interactions. *Chem. Soc. Rev.* **2010**, *39*, 4195−4205.
(17) Xu, B.; Tao, N. Measurement of Single-Molecule Resistance by Repeated Formation of Molecular Junctions. *Science* **2003**, *301*, 1221−1223.
(18) Xiang, D.; Wang, X.; Jia, C.; Lee, T.; Guo, X. Molecular-Scale Electronics: From Concept to Function. *Chem. Rev.* **2016**, *116*, 4318−4440.
(19) Yang, C.; Yang, C.; Guo, Y.; Feng, J.; Guo, X. Graphene-Molecule-Graphene Single-Molecule Junctions to Detect Electronic Reactions at the Molecular Scale. *Nat. Protoc.* **2023**, *18*, 1958−1978.
(20) Yang, C.; Qin, A.; Tang, B.; Guo, X. Fabrication and Functions of Graphene-Molecule-Graphene Single-Molecule Junctions. *J. Chem. Phys.* **2020**, *152*, 120902.
(21) Ayinla, R. T.; Shiri, M.; Song, B.; Gangishetty, M.; Wang, K. The Pivotal Role of Non-Covalent Interactions in Single-Molecule Charge Transport. *Mater. Chem. Front.* **2023**, *7*, 3524−3542.
(22) Frisenda, R.; Janssen, V. A.; Grozema, F. C.; van der Zant, H. S.; Renaud, N. Mechanically Controlled Quantum Interference in Individual π-Stacked Dimers. *Nat. Chem.* **2016**, *8*, 1099−1104.
(23) Li, P.; Hou, S.; Alharbi, B.; Wu, Q.; Chen, Y.; Zhou, L.; Gao, T.; Li, R.; Yang, L.; Chang, X.; et al. Quantum Interference-Controlled Conductance Enhancement in Stacked Graphene-Like Dimers. *J. Am. Chem. Soc.* **2022**, *144*, 15689−15697.
(24) Feng, A.; Zhou, Y. M.; Al-Shebami, A.; Chen, L.; Pan, Z.; Xu, W.; Zhao, S.; Zeng, B.; Xiao, Z.; Yang, Y.; et al. σ-σ Stacked SupraMolecular Junctions. *Nat. Chem.* **2022**, *14*, 1158−1164.
(25) Su, T. A.; Li, H.; Steigerwald, M. L.; Venkataraman, L.; Nuckolls, C. Stereoelectronic Switching in Single-Molecule Junctions. *Nat. Chem.* **2015**, *7*, 215−220.
(26) Xin, N.; Wang, J.; Jia, C.; Liu, Z.; Zhang, X.; Yu, C.; Li, M.; Wang, S.; Gong, Y.; Sun, H.; et al. Stereoelectronic Effect-Induced Conductance Switching in Aromatic Chain Single-Molecule Junctions. *Nano Lett.* **2017**, *17*, 856−861.
(27) Meng, L.; Xin, N.; Wang, J.; Xu, J.; Ren, S.; Yan, Z.; Zhang, M.; Shen, C.; Zhang, G.; Guo, X.; Meng, S.; et al. Atomically Precise Engineering of Single-Molecule Stereoelectronic Effect. *Angew. Chem., Int. Ed.* **2021**, *60*, 12274−12278.
(28) Raju, R. K.; Bloom, J. W.; An, Y.; Wheeler, S. E. Substituent Effects on Non-Covalent Interactions with Aromatic Rings: Insights from Computational Chemistry. *ChemPhysChem* **2011**, *12*, 3116−3130.
(29) Chen, H.; Stoddart, J. F. From Molecular to Supramolecular Electronics. *Nat. Rev. Mater.* **2021**, *6*, 804−828.
(30) Li, P.; Chen, Y.; Wang, B.; Li, M.; Xiang, D.; Jia, C.; Guo, X. Single-Molecule Optoelectronic Devices: Physical Mechanism and Beyond. *Opto-Electron. Adv.* **2022**, *5*, 210094.
(31) Kilgore, H. R.; Raines, R. T. $\pi \rightarrow \pi^*$ Interactions Modulate the Properties of Cysteine Residues and Disulfide Bonds in Proteins. *J. Am. Chem. Soc.* **2018**, *140*, 17606−17611.
(32) Glendening, E. D.; Landis, C. R.; Weinhold, F. Natural Bond Orbital Methods. *Wiley Interdiscip. Rev. Comput. Mol. Sci.* **2012**, *2*, 1−42.
(33) Solomon, G. C.; Herrmann, C.; Hansen, T.; Mujica, V.; Ratner, M. A. Exploring Local Currents in Molecular Junctions. *Nat. Chem.* **2010**, *2*, 223−228.
(34) Solomon, G. C.; Herrmann, C.; Vura-Weis, J.; Wasielewski, M. R.; Ratner, M. A. The Chameleonic Nature of Electron Transport through π-stacked Systems. *J. Am. Chem. Soc.* **2010**, *132*, 7887−7889.
(35) Yanson, A. I.; Bollinger, G. R.; van den Brom, H. E.; Agraït, N.; van Ruitenbeek, J. M. Formation and Manipulation of a Metallic Wire of Single Gold Atoms. *Nature* **1998**, *395*, 783−785.
(36) Burns, J. A.; Butler, J. C.; Moran, J.; Whitesides, G. M. Selective Reduction of Disulfides by Tris(2-carboxyethyl)phosphine. *J. Org. Chem.* **1991**, *56*, 2648−2650.
(37) Adak, O.; Rosenthal, E.; Meisner, J.; Andrade, E. F.; Pasupathy, A. N.; Nuckolls, C.; Hybertsen, M. S.; Venkataraman, L. Flicker Noise as a Probe of Electronic Interaction at Metal-Single Molecule Interfaces. *Nano Lett.* **2015**, *15*, 4143−4149.
(38) Yuan, S.; Gao, T.; Cao, W.; Pan, Z.; Liu, J.; Shi, J.; Hong, W. The Characterization of Electronic Noise in the Charge Transport through Single-Molecule Junctions. *Small Methods* **2021**, *5*, 2001064.
(39) Pan, Z.; Chen, L.; Tang, C.; Hu, Y.; Yuan, S.; Gao, T.; Shi, J.; Shi, J.; Yang, Y.; Hong, W. The Evolution of the Charge Transport Mechanism in Single-Molecule Break Junctions Revealed by Flicker Noise Analysis. *Small* **2022**, *18*, 2107220.
(40) Baker, T. A.; Friend, C. M.; Kaxiras, E. Nature of Cl Bonding on the Au(111) Surface: Evidence of a Mainly Covalent Interaction. *J. Am. Chem. Soc.* **2008**, *130*, 3720−3721.

https://doi.org/10.1021/acsmaterialslett.4c00402
ACS Materials Lett. 2024, 6, 1961−1967